Electrospinning of Polyacrylonitrile Solutions at Elevated Temperatures

Chi Wang,* Huan-Sheng Chien, Chia-Hung Hsu, Yin-Chi Wang, Cheng-Ting Wang, and Hsin-An Lu

Department of Chemical Engineering, National Cheng Kung University, Tainan 701, Taiwan, ROC

Received March 1, 2007; Revised Manuscript Received August 21, 2007

ABSTRACT: Using a jacket-type heat exchanger to control the solution temperature, the electrospinning of polyacrylonitrile/dimethylformamide (PAN/DMF) solutions with various concentrations was carried out at temperatures ranging from ambient to 88.7 °C. The purpose of this is to investigate the temperature effect on the cone/jet/fiber morphologies that developed. By varying the solution temperature, the chain entanglement status existing in the solution (which is the prerequisite condition for preparing uniform fibers) remained intact. However, the solution properties were significantly altered, thereby giving rise to a feasible route to manipulate the as-spun fiber diameter. By increasing the solution temperature, it was found that the viscosity (η_o) and surface tension (γ) of the PAN/DMF solutions were decreased, but the solution conductivity (κ) was increased; all these trends favored the development of thinner electrospun PAN fibers at high electrospinning temperatures. For instance, with the 6 wt % solutions, PAN fibers with a diameter of 65−85 nm were readily prepared by electrospinning at 88.7 °C, whereas larger fibers with a diameter of 190−240 nm were frequently obtained at room temperature. The temperature dependence of η_o, γ, and κ followed the Arrhenius equation, and the corresponding activation energies were composition dependent and found to be ca. 15−28, ∼10 and ∼3.7 kJ/mol, respectively. High-temperature electrospinning eventually produced PAN fibers with less crystallinity but higher chain orientation as revealed by the wide-angle X-ray diffraction and birefringence measurements. Moreover, the scaling law for the viscosity dependence of fiber diameter, d_f, was also altered from $d_f = 14.8\eta_o^{0.52}$ (unit: d_f in nm and η_o in cP) at room temperature to $d_f = 3.0\eta_o^{0.74}$ at 88.7 °C, suggesting that high-temperature electrospinning was an effective method to produce ultrathin fibers.

1. Introduction

Similar equipment consisting of a solution delivery system, a pendent drop with Taylor cone meniscus, a high electric field, and a grounded collector are involved in the electrospraying and electrospinning processes.[1−4] Due to the distinct differences in solution rheology, however, electrospraying produces spherical particulates resulting from the capillary breakup of the electrified jet, whereas electrospinning gives uniform (bead-free) fibers resulting from the electrostatic jet stretching associated with the surface charge repulsion in the bending instability region.[5−7] The prerequisite for fiber formation is the presence of sufficient chain-entanglement density in the working solution to develop a deformable network, therefore preventing the capillary breakup.[8−10] In other words, there exists a minimum concentration (C_{min}) below which entanglements of polymer chains are absent, and electrospinning will degenerate to electrospraying. On the other hand, polymer solutions with a concentration of C_{min} sometimes possess a sufficiently high viscosity (ca. 100 cP, depending upon the polymer/solvent pair). This leads to difficulties in preparing electrospun fibers with a diameter less than 100 nm. Thus, several approaches have been proposed to resolve this problem. By adding a soluble salt[11,12] or a more conductive solvent,[13] the solution conductivity can be effectively enhanced to eliminate the beaded fibers structure, which is frequently observed in electrospinning polymer solutions with insufficient entanglement density. Benefits may be also obtained from the reduction of solution viscosity due to salt addition, but salt extraction from the electrospun fibers is sometimes required for further application. The understanding

of the sophisticated interaction of this polymer/solvent/salt system is crucial for a reproducible process control. The second method is to use polymer species which have an ultrahigh molecular weight (UHMW) on the basis of a simple relation:[14] $C_{min} \sim 2M_e/M$, where M_e is the entanglement molecular weight in melt dependent on the polymer types,[15,16] and M is the molecular weight of the polymers used for electrospinning. Using UHMW polymers, the C_{min} is lowered, and the corresponding viscosity is effectively reduced for obtaining small-diameter fibers.[15,17] Depending on the synthesis techniques, however, the UHMW species are not readily available for most polymers. The third method is to use a coaxial tube as a spinneret[18,19] in which two polymer solutions with appropriate properties are fed into the core and sheath regions, respectively. The desired polymer solution with a concentration lower than C_{min} (low viscosity) is fed into the inner tube, and the resulting core jet is stabilized and protected by the shell solution during jet bending. In this manner, the composite fibers with core/shell structures are successfully collected. Afterward, the outer layer is removed by selective solvent dissolution to obtain the core fibers with a diameter less than that prepared by a single-duct spinneret using a single fluid of C_{min}. Two different solutions are involved in the coaxial electrospinning process, and the relative ratios of the flow rate and properties of these two solutions are critical in controlling the desired diameter of the electrospun fibers. Although this approach has quite a potential in practical applications, it is not an easy task at present to search for the appropriate processing conditions for electrospinning.

All previous results demonstrated that solution viscosity is the most important factor in determining the diameter of the electrospun fibers; the lower the solution viscosity, the thinner

---

* Corresponding author. Fax: +886-6-2344496. Telephone: +886-6-2757575, Ext 62645. E-mail: chiwang@mail.ncku.edu.tw.

the electrospun fibers.[8,9,11,13,14,20–22] It is well-known that solution viscosity is effectively reduced at higher temperatures; however, the chain entanglement status is relatively independent of the solution temperature. On the basis of these two facts, the obtainment of ultra-fine fibers is likely by simply carrying out the electrospinning of solutions having a concentration of C_{min} at high temperatures. Moreover, high-temperature electrospinning is essentially required in those cases in which significant intermolecular-chain association takes place and/or no common solvents are readily available at room temperature for making homogeneous solutions for electrospinning. For instance, Li et al.[23] succeeded in preparing gelatin fibers by electrospinning an aqueous gelatin solution at 40 °C, which was above its gelation temperature (~37 °C). In contrast, the difficulties are often encountered when room-temperature electrospinning of aqueous gelatin solution is conducted. It is attributable to the presence of gelation phase transition. Although a lower level of gelation may assist in the uniform fiber formation for electrospinning at a concentration lower than C_{min},[24] at least in part due to the partial network formation, the as-spun fiber morphologies are difficult to control. On the other hand, excessive gelation usually leads to the blockage of the Taylor cone. In addition, some semicrystalline polymers (e.g., poly-ethylene, polypropylene) are dissolved in solvents only at elevated temperatures. This suggests the urgent importance for developing a high-temperature electrospinning apparatus. A recent study on the electrospinning of linear low-density polyethylene at a temperature of 110 °C has been reported by Givens et al.[25] In spite of its importance, however, no detailed experimental data regarding the temperature effect have been stated until now in the literature on cone/jet/fiber morphologies during the solution electrospinning process.

Being the precursor for high-performance carbon fiber, polyacrylonitrile (PAN) fibers are of importance. PAN-based carbon fibers essentially dominate consumption by accounting for nearly 90% of carbon fiber sales worldwide compared with the pitch-based or vapor-grown fibers. It is generally believed that the main drawback of prolonged time required for the thermal conversion of PAN fibers into structural carbon fibers can be greatly resolved if the fiber diameter is significantly reduced.[26] Driven by the motivation of nanofiber preparation, many researchers[26–39] have worked on the electrospinning of PAN/DMF solutions and have obtained electrospun PAN diameters in the range of 200–15000 nm depending on the spinning conditions. While significant insights have been achieved, there are still many unresolved issues and inconsistent results among the different research works, and these need to be carefully addressed and discussed. Most of the previous work has paid much attention on the relation between the processing variables and the electrospun fiber morphology, thereby leaving the important issue of the free surface variations largely unexplored. In addition, there have been difficulties encountered in preparing PAN fibers with a diameter lower than 100 nm using room-temperature electrospinning, as mentioned previously.[18]

The aim of this work is to achieve a complete understanding of the temperature factors affecting the cone/jet/fiber morphologies during the electrospinning of PAN/DMF solutions via the variations of solution properties and processing variables (flow rate, working distance, and applied voltage). For comparison, we carried out room-temperature electrospinning as a first step to acquire the concentration dependence of Taylor cone volume, jet length, jet diameter, bending instability, and fiber morphology. The results obtained were discussed and compared with

previously reported data in order to obtain a more comprehensive and consistent picture of PAN/DMF electrospinning. The viscosity dependence of fiber (jet) diameter was discussed, and an attempt was made to obtain the C_{min} required for preparing uniform electrospun fibers. In the second part, the temperature effects on the solution properties, e.g., viscosity, conductivity, and surface tension, were investigated, and the corresponding activation energies were derived. In the final part, high-temperature electrospinning was conducted at various temperatures, and the temperature effects on the cone/jet/fiber morphologies as well as the birefringence and crystallinity of the collected PAN fibers were reported. Our results suggested that PAN nanofibers with a diameter of ~65 nm were readily obtained by means of electrospinning at 88.7 °C. Moreover, as opposed to electrospinning at room temperature, a stronger viscosity dependence of fiber diameter was recognized due mainly to the enhanced solution properties at high temperatures, that is, higher conductivity and lower surface tension.

2. Experimental Section

2.1. Solution Preparation and Properties. The PAN powders purchased from Aldrich Co. were used, and dimethylformamide (DMF) obtained from J.T. Baker (HPLC grade) was applied as a solvent. Using the Huggins Equation, the intrinsic viscosity [η] at 25 °C was determined to be 186.1 mL/g, which corresponded to a viscosity average molecular weight (M_v) of 141 400 g/mol calculated from the relationship of $[\eta] = 52 \times 10^{-3} M_v^{0.69}$.[40] The solubility parameters were 12.5 and 12.1 (cal/cm^3)$^{0.5}$ for PAN and DMF respectively, which suggested that DMF was a good solvent for PAN. In order to prepare solutions with different weight percent concentrations, weighted amounts of polymers and solvents were mixed for several hours until homogeneous solutions were obtained. Filtration and degassing were occasionally performed to remove the impurity and small bubbles in the solution. Using the density values of 1.184 and 0.944 g/cm^3 for PAN and DMF respectively, the conversion of weight percent to volume percent for as-prepared solutions was performed. To enhance the solution conductivity, triethylbenzylammonium chloride (TEBAC) salt was added, and the salt concentration was relative to the mass of the solvent used. Solution properties like conductivity (κ), surface tension (γ), and viscosity (η_o) were measured at various temperatures. The surface tension, conductivity, and viscosity of the prepared solutions were measured using the Face surface tension meter (CBVP-A3), Consort conductivity meter (C832), and Brookfield viscometer (LVDV-I+, spindle 18, and cup 13R), respectively. The linear viscoelastic properties of the solutions were measured in a Rheometrics (ARES) using a cup-and-bob feature. The oscillatory shear mode was used to determine the storage modulus $G'(\omega)$ and loss modulus $G''(\omega)$ over a range of frequencies. Zero shear viscosity η_o was determined from the loss modulus data at low frequencies: $\eta_o = \lim_{\omega \to 0} G''(\omega)/\omega$. Recoverable shear compliance J_s^o was determined from the storage modulus data at low frequencies: $J_s^o = 1/\eta_o^2 \lim_{\omega \to 0} G'(\omega)/\omega^2$. The relaxation time τ_o was estimated by: $\tau_o = \eta_o J_s^o$.[41]

2.2. Processing and Measurements. Figure 1 shows the schematic diagram of the high-temperature electrospinning system. A homemade jacket-type heat exchanger was used to maintain the polymer solution at a desired temperature for electrospinning. The circulation of heated silicone oil was fulfilled by a pumping system connected to an oil bath where a temperature up to 130 °C could be adjusted. A significant temperature gradient was found along the needle due to its "one-dimensional fin" geometry, thereby giving rise to an apparent temperature difference for solutions within the jacket tube and those within the electrified Taylor cone. By measuring the temperature of the pendant drop at the needle end using a thermocouple, the solution working temperature for electrospinning was determined. To ensure a continuous spinning process, a saturated DMF steam at a predetermined temperature was delivered using a controlled flow rate of N$_2$ carrier gas to
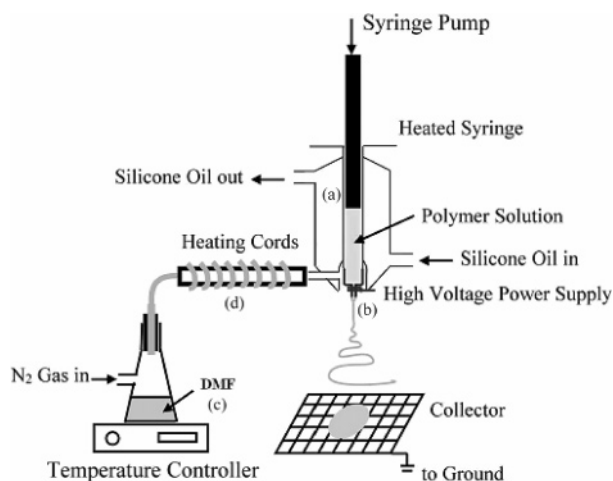
Figure 1. Schematic setup of the high-temperature electrospinning apparatus: (a) a jacket-type heat exchanger used for maintaining the polymer solution at a constant temperature controlling by the circulating heated silicone oil, (b) a needle where a high voltage is applied and high-temperature saturated DMF vapor is introduced to encapsulate the Taylor cone to eliminate the jet interruption, (c) DMF vapor generator using N_2 as the carrier gas, and (d) a heating device to maintain the vapor temperature for resolving the DMF condensation problem.

blanket the Taylor cone. This is done without interrupting the bending instability. It should be noted that solvent evaporation may be significantly enhanced when the solution temperature approaches the boiling temperature of the solvent used (153 °C for DMF). This would result in gradual cone shrinkage and lead to unstable electrospinning. For our designed apparatus, a stable cone-jet electrospinning could be performed smoothly on the PAN/DMF solutions at a temperature up to 88.7 °C. When the system reached a thermal equilibrium, the homogeneous polymer solution was delivered by a syringe pump (Cole-Parmer) at a controlled flow rate (Q, typically 0.3 mL/h) to the needle (o.d. = 1.47 mm, unless otherwise indicated), where a high electrical voltage (typically 6–10 kV) was applied by a high-voltage source (Bertan, 205B). Needles with different sizes were also tested to reveal their effect on the electrospinning. In order to construct a point-to-plate electrode configuration, a steel net (30 × 30 cm²) was used as a collector for the electrospun fibers at a working distance (H) of 7.0 cm below the needle tip. Four CCDs were used to observe the electrospinning process during the experiments: CCD1 (Sony XC77) for the shape variation of the Taylor cone at the needle tip, CCD2 (Sony CCDTRV53) for the liquid jet emitting from the Taylor cone bottom due to the electric repulsion, and CCD3 for the bending instability envelope. CCD3 is a high-speed camera (Redlake, Motion Pro 10000) used to capture an image at a frame rate of 10000 frame/s. Laser diffraction was used to monitor the diameter variation of liquid jet from the Taylor cone bottom to the point where bending instability took place. A 1 mW He–Ne laser with a pinhole of 1 mm diameter was used as a light source, and the diffraction patterns on the screen were collected by CCD4 (Sony XC77) and further analyzed by the Inspector software. The liquid jet diameters (d_j), just prior to the bending instability were determined by the first maximum diffracted intensity using $d_j = 1.43\lambda X/Y$, where λ is the wavelength of the laser light (632.8 nm), X is the distance from the jet to the screen, and Y is the distance between the beam center and the first intensity maximum.[42]

The morphology and diameter of the electrospun fibers were observed using a scanning electron microscope (SEM, Hitachi S4100). The fiber diameters were measured within SEM micrographs from a population of ~500 fibers from which the average fiber diameter (d_f) and the corresponding standard error were determined. The birefringence of individual fibers collected on the glass slide was measured using a polarized optical microscope (Lica Co., DMLP) equipped with a tilting compensator (Leitz Co.). To characterize the fiber crystallinity, wide-angle X-ray diffraction

(WAXD) patterns were obtained using a RINT2000 X-ray goniometer (Rigaku, Cu target) operated at 40 kV and 30 mA with a 2θ scan speed of 1°/min and sampling width of 0.05°. The crystallinity fraction (ϕ^{WAXD}) of the crystallized samples was determined from the area ratio of the resolved crystalline peaks to the unresolved total scattering curve. The thermal properties and stability of the electrospun fibers were analyzed using a Perkin-Elmer differential scanning calorimeter (DSC7) and TA Instrument thermogravimetric analyzer (TGA, Q500) at a heating rate of 10 °C/min under nitrogen.

In this study, the effects of applied voltage (V), flow rate (Q), polymer volume fraction (ϕ), and salt addition on the electrospinning process were discussed.

3. Results and Discussion

3.1 Room-Temperature Electrospinning. Being a nonsolvent to PAN,[43,44] the water vapor adjacent to the Taylor cone would interact with the PAN/DMF solution to form a coagulation on the cone surface, consequently affecting the stable jet formation and fiber reproducibility, especially for a highly humid atmosphere. The presence of moisture in the bending instability region might also reduce the effectiveness of jet stretching and interfere with the fiber morphology. To resolve this problem, a gas jacket[45] was used for introducing N_2 to blanket the Taylor cone, the purpose of which was to eliminate moisture attack. It should be noted, however, that a sufficient N_2 flow rate was required, without interrupting the jet bending, to appropriately encapsulate the Taylor cone during electrospinning. In the absence of the N_2 purge, the electrospun fiber diameter was found to be slightly larger than that obtained with the N_2 purge; the difference was evident for the concentrated PAN solutions used at a high humidity but became diminished for the low PAN concentrations (e.g., <8 wt %) at a low humidity (e.g., <40%). Interestingly, Yoon et al.[46] found that the diameter of the electrospun PAN fibers increased with an increase in PAN concentration, but became leveled off at a concentration higher than 10 wt %. To exclude the data variations associated with moisture interaction, an N_2 purge was always used during room-temperature electrospinning.

C_{min} **Determination.** A sufficient entanglement density existing in the electrospinning solution is an important requirement (a sufficient but not necessary condition as pointed out recently by Yu et al.[47]) for developing uniform electrospun fibers. On the basis of the method proposed by McKee et al.,[8] the log–log plot of the solution specific viscosity (η_{sp}) vs volume fraction (ϕ) is shown in Figure 2a to determine the C_{min} required for uniform PAN fibers electrospun. The concentration dependence of η_{sp} is found to change from $\eta_{sp} \sim \phi^{1.0}$ for a dilute solution to $\eta_{sp} \sim \phi^{4.78}$ for solutions possessing entangled chains. C_{min} is determined to be ~5 wt %, at which the final linear domain is first seen. This indicates the transition from the unentangled to the entangled regime. For higher concentrations, all data fall on the straight line with a constant slope of 4.78. The solution regime transition was accompanied by a morphological variation of electrospun products, that is, micrometer-sized PAN particulates were obtained from solutions with PAN concentrations lower than 4 wt %, fiberlike structures (beaded fibers) were first seen in the 5 wt % solution, and finally, uniform PAN fibers were readily prepared from the 6 wt % (or higher) solution. Our results were in accordance with previous findings by McKee et al.[8] on the electrospinning of PET solutions and those by Wang et al.[39] on using PAN copolymer solutions. Figure 2b shows the ϕ dependence of J_s^o where a power law relation of $J_s^o \sim \phi^{1.9}$ is seen. The derived exponent is close to the theoretical value (~2.0) for solutions with
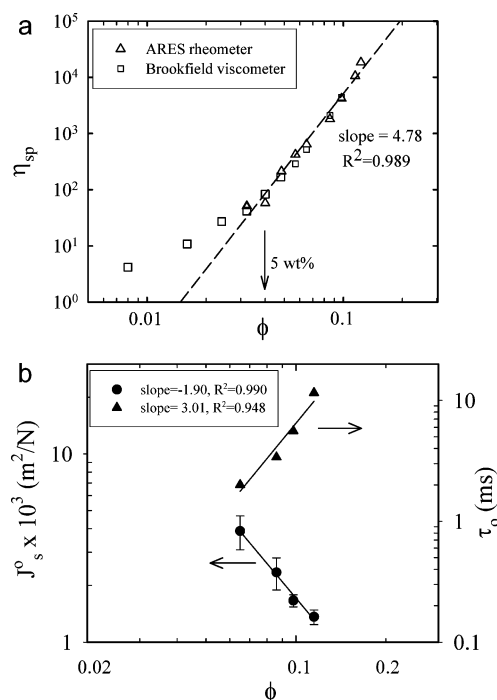
Figure 2. (a) Typical plot of specific viscosity, η_{sp}, vs volume fraction of PAN, ϕ, at ambient temperature. The deviation of the final straight line is starting at the 5 wt % solution, where the incipient concentration for the chain entanglement is estimated, (b) ϕ dependence of J_s^o and τ_o for PAN/DMF solutions under ambient conditions.

entangled mono-dispersed polymeric chains,[48] suggesting that the entangled regime is reached for PAN concentrations larger than 6.5 vol % (or 8 wt %). For PAN concentrations lower than 8 wt %, however, the inability to obtain a reliable G' is due to the constraints of torque measurements, which in turn leads to the infeasibility of J_s^o measurements. In consideration of the difficulty in identifying the J_s^o measurements for dilute solutions, it seems that Figure 2a provides a more accessible determination of C_{min} as opposed to using the $\log J_s^o - \log \phi$ plot together with the slope identification changing from 1.0 for the unentangled regime to 2.0 for the entangled regime.[48] Nevertheless, the determination of J_s^o seems inevitable for the estimation of the relaxation time of polymeric chains, which is important in characterizing electrospinnability as pointed out by Yu et al.[47] Also given in Figure 2b are the values of τ_o derived by the product of J_s^o and η_o. It shows that τ_o increases from 2 ms for the 6.5 vol % solution to 11.6 ms for the 11.5 vol % solution, and that it follows a power law relation of $\tau_o \sim \phi^{3.0}$.

Although the experimentally determined M_e for the PAN melt is not available yet, a simple relation proposed by Wool[15] for estimating M_e is expressed as $M_e \sim 15C_\infty M_o$, where C_∞ is the characteristic ratio and M_o is the monomer molecular weight. With a reported C_∞ value of 9.7,[40] the derived M_e for the PAN melt is ca. 7700 g/mol, which gives a theoretically predicted C_{min} value of 10.9 vol % (or 13.3 wt %). In contrast with the much lower C_{min} value ($\sim$4 vol %) obtained from Figure 2a, this indicates that there exists a strong association between the PAN chains and DMF solvents in the solution state,[44] significantly reducing the entanglement concentration.

Functioning Domains and Effects of Flow Rate and Solution Properties. For a given PAN/DMF solution at a fixed H, the functioning domain defined by the operating voltage (V) range and flow rate (Q) for the stable cone−jet electrospinning mode was first determined. Figure 3 shows the typical $V-Q$
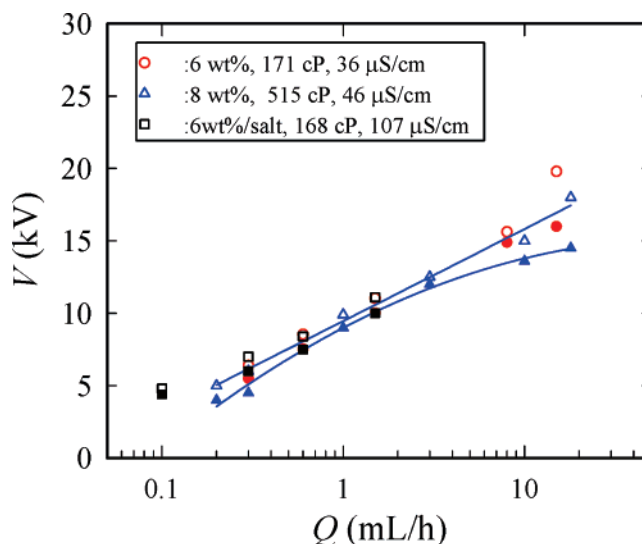

Figure 3. Typical functioning domains showing the range of operating voltage required for the stable cone−jet spinning mode; filled symbols for the lower bond voltage, V_s, and open symbols for the upper bound voltage, V_{us}. Solid lines are the eye-guide of the processing window for the 8 wt % PAN solution. The solution viscosity is changed by PAN wt%, the conductivity is varied by 0.05 wt % TEBAC addition, but the surface tension is unchanged at 36.3 dyn/cm regardless of PAN and salt contents. $H = 7.0$ cm. The o.d. of needle is 1.47 mm.

relations for the 6 and 8 wt % PAN solutions, where the filled symbols represent the lower bound V_s and the open symbols give the upper bound V_{us} for the stable electrospinning with a single electrified jet. For an applied voltage lower than V_s, dripping of the solution drop is still observed.[14] On the other hand, for an applied voltage higher than V_{us}, two jets might develop in some occasions, issuing steadily from the electrified cone. Multiple-jet electrospinning has also been observed in the polystyrene (PS)/terahydrofuran/salts[14] and polyurethaneurea/DMF solutions.[21] The formation of multiple jets under a high electric field is attributed to the presence of excess surface charge on the electrified cone associated with the high conductivity and mobility of the solutions. Depending on the processing variables (Q, H, and V), the number of jets was varied and associated with the dynamics of the free surface cone whose size was balanced by the inlet flow from the supplying line, the outlet flow through the jet line due to the electric field strength, and the adhering force at the needle end for suspending the cone. For a solution with a high κ and a low η_o (i.e., low PAN contents with salt additions), the jet number was significantly dependent on the flow rate applied. For example, the electrospinning of the 6 wt % solutions with 0.05 wt % TEBAC under a processing condition of 2 mL/h and 14.2 kV yielded nine jets to produce fibers with a diameter of 247 ± 49 nm; in comparison, four jets were seen at 6 mL/h and 19.7 kV to give a fiber diameter of 222 ± 36 nm. It was found that a cone with multiple jets (cone−jets electrospinning) did not warrant producing thinner electrospun fibers than that containing a single jet (cone−jet electrospinning). For simplicity and concise comparison, single jet electrospinning will be exclusively addressed in the following sections; thus the processing window for the 8 wt % PAN solution is defined by the solid lines as shown in Figure 3.

Changing the PAN solutions from 6 to 8 wt % led to an increase of η_o from 171 to 515 cP, together with a slight increase of κ from 36 to 46 μS/cm. The κ effect on the functioning domain was also investigated by adding 0.05 wt % TEBAC into the 6 wt % solution to enhance the conductivity to 107 μS/cm, accompanied by a small decrease of η_o to 168 cP. For

Table 1. Effects of Conductivity, Flow-Rate, and Applied Voltage on the Cone/Jet/Fiber Dimensions (Room-Temperature Electrospinning)[a]

solution	Q (mL/h)	cone height (mm)	jet length (mm)	d_j (μm)	d_f (nm)	l_f/l_j
6 wt %	0.3	1.49	2.24	3.25 ± 0.19	240 ± 81	8.8
	0.6	1.41	2.21	5.31 ± 0.27	194 ± 36	35.9
	1.5	1.52	2.64	7.25 ± 0.25	203 ± 45	61.3
8 wt %	0.3	1.49	2.80	4.04 ± 0.20	353 ± 71	8.5
	0.6	1.54	2.90	6.20 ± 0.86	292 ± 37	29.2
	1.5	1.49	2.95	7.52 ± 0.39	298 ± 59	41.4
6 wt % with salt	0.3	1.60	2.13	3.92 ± 0.12	255 ± 41	11.4
	0.6	1.60	2.75	5.64 ± 0.26	194 ± 31	40.5
	1.5	1.67	2.85	7.39 ± 0.16	198 ± 40	66.5

[a] Note: For all solutions, the applied voltages for Q = 0.3, 0.6, and 1.5 mL/h are 6.0, 7.8, and 9.7 kV, respectively; thus the nominal electric strengths are 0.86, 1.11, and 1.39 kV/cm. The o.d. of the needle is 1.47 mm.

these solutions, the surface tension remained identical at 36.3 dyn/cm, but a factor of 3 differences in the η_o (or κ) was found among one another. As shown in Figure 3, at a given Q, the voltage for the cone−jet electrospinning is relatively independent of η_o and κ, and a rather limited range is available (only ~1 kV at a lower Q). For a given solution, on the other hand, the voltage for the cone−jet electrospinning mode is significantly increased with an increase in Q. For instance, 4.0−5.0 kV is required for electrospinning the 8 wt % solution at a flow rate of 0.2 mL/h, but it rises to a voltage of 14.5−18.0 kV at a flow rate of 18.0 mL/h. The effects of η_o and κ on the applied V required for electrospinning are slightly different from those observed for the less conductive PS/DMF solutions,[14] suggesting the importance of functioning domain determination prior to the experimental scheme design in order to explore the individual parameter (η_o, κ, Q) influence on the spinning process.

According our previous study on PS solutions,[14] Q is a convenient variable for manipulating the fiber diameter, that is, thinner fibers are obtained by a smaller Q provided that the other two processing variables (H and V) are fixed. The Q effects on the cone/jet/fiber morphologies are shown in Table 1. According to Figure 3, it seemed impossible to apply a fixed V for investigating the Q effects on the electrospinning process for a fair comparison; therefore, the applied V was set at 6.0, 7.8, and 9.7 kV respectively for a flow rate of 0.3, 0.6, and 1.5 mL/h. As Q was increased from 0.3 to 1.5 mL/h for electrospinning of the 6 wt % solution, the cone height and jet length were relatively unchanged, d_j was evidently increased, and d_f was reduced from 240 to 203 nm. Similar Q dependences of the cone/jet/fiber morphologies were also found for the other two solutions. A simple relation between d_j and Q was obtained,[49] $d_j \sim Q^n$ with n ranging from 0.35 to 0.39, for all the three solutions used. The scaling exponent is slightly lower than the previously derived one (~0.5) for the PS solutions,[14,49] and this is plausibly due to the difference in the electric field applied. Although d_j is larger for a larger Q, the apparent d_f reduction is attributed to an enhanced electric strength resulting from a higher V used. In other words, for the present PAN solutions, the applied V becomes a more dominant parameter in determining fiber diameter than Q; this is a striking difference from the electrospinning of PS solutions where Q is the key controlling factor due to its less conductive nature.[14]

As far as the solution properties are concerned, viscosity plays a more dominant role than the conductivity in determining the fiber diameter, which is consistent with previous results.[14] As shown in Table 1, despite the 3-fold enhancement of κ due to

the presence of salts, d_f is found unchanged in comparison with that without adding salt; on the other hand, the d_f obtained from the 8 wt % solution is evidently increased due to three times of η_o increase. Also given in Table 1 is the draw ratio (l_f/l_j, where l_j and l_f are the phantom length of the jet and fiber, respectively) associated with the jet stretching in the bending instability region, which was determined by a simple relation: $l_f/l_j \sim (d_j/d_f)^2\phi$, based on the assumption of volume conservation. The calculated l_f/l_j ratio is increased with an increase in Q which is attributable to the presence of a higher electric field for a larger Q. It is of interest to note that the draw ratio is as high as 60 for Q = 1.5 mL/h, in contrast with the electrospinning of PS solutions which gives a draw ratio of ca. 2.5 under a similar electrospinning condition. The presence of a much higher draw ratio suggests a more severe stretching during jet bending deformation, which in turn produces finer electrospun fibers. As a matter of fact, PS fibers with a diameter of several micrometers are frequently obtained; in comparison, submicrometer-sized PAN fibers are readily prepared from the room-temperature electrospinning process.

Effects of Needle Diameter. Although intensive research efforts have been devoted to parameter (Q, H, V, η_o, κ, and γ) effects on the electrospinning process,[12−14,20−23,26,30,39] the effect of needle (capillary) diameter is barely discussed in the literature.[30] To reveal the needle diameter effect on the cone/jet/fiber morphologies, three different needles were used to electrospin the 8 wt % solution under the same processing conditions. The results are shown in Table 2. The needle end was completely wetted during electrospinning by the protruded pendant drop, which implies the importance of outer diameter for comparison. As shown in Table 2, the size of the Taylor cone and the electrified jet are apparently increased with an increase in needle diameter. Despite the five times difference in the needle diameter, the jet diameter was constant (ca. 4.0 μm). However, the fiber diameter was found to increase from 256 to 502 nm, accompanied by a lower drawability and less birefringence, when the needle diameter was increased from 0.57 to 2.77 mm. Because of the point-to-plate electrode configuration, the electric field close to the Taylor cone is essentially nonuniform, and its field strength is significantly higher than the nominal strength, E_o, determined by V/H. The nonuniformity of the electric field can be experimentally realized from the absence of intimate superposition between the obtained d_f and V/H by varying either V or H and leaving the other constant.[14,39]

To estimate the electric field near the needle end, simple finite element analysis (FEA) was carried out.[50] In the absence of electrospinning fluids (an empty hollow needle), Figure 4a shows the calculated strength of electric field as a function of distance from the needle end (z = 0 mm) to the grounded plate (z = 70 mm) along the symmetry line. For the three needles investigated, the locations of jet ends are marked by the filled symbols, and the corresponding electric field strength (E_j/E_o) is then determined and tabulated in Table 2. As shown in the inset of Figure 4a, the electric field for the point-to-plate configuration is not uniform at all. A significant concentration of the electric field is found at the needle end, and the field strength is decreased with an increase in distance followed by a simple relation: $E/E_o \sim (z/R_o)^{-1.21}$, where R_o is the outer diameter of the needle.

To reveal the electrospinning fluid effect on the electric field, a stagnant solution with a relative permittivity of 36.7 (for the DMF solvent) was considered, and the FEA results are displayed in Figure 4b with an inset showing the axisymmetric model studied. In the inset, the shaded area represents the stagnant

Table 2. Effects of Needle Diameter on the Morphologies of the Electrified Cone and Jet as Well as the Electrospun Fibers (Room-Temperature Electrospinning)^a

needle code	i.d/o.d. (mm)	cone height (mm)	jet length (mm)	d_j (μm)	d_f (nm)	l_f/l_j	$\Delta n \times 10^2$	$E_j/E_o{}^b$
ND−S	0.31/0.57	0.88	2.42	4.08 ± 0.07	256 ± 40	16.5	6.0	2.82
ND−M	1.07/1.47	0.94	4.30	3.99 ± 0.04	308 ± 54	10.9	5.0	2.15
ND−B	2.16/2.77	1.48	7.00	4.10 ± 0.09	502 ± 48	4.3	3.0	1.47

^{a} 8 wt % PAN/DMF solutions were used and the processing variables were fixed at $Q = 0.2$ mL/h, $H = 7$ cm, and 5.0 kV. ^{b} E_j is the calculated electric strength at the jet end and E_o is the nominal electric strength, 71.4 kV/m.
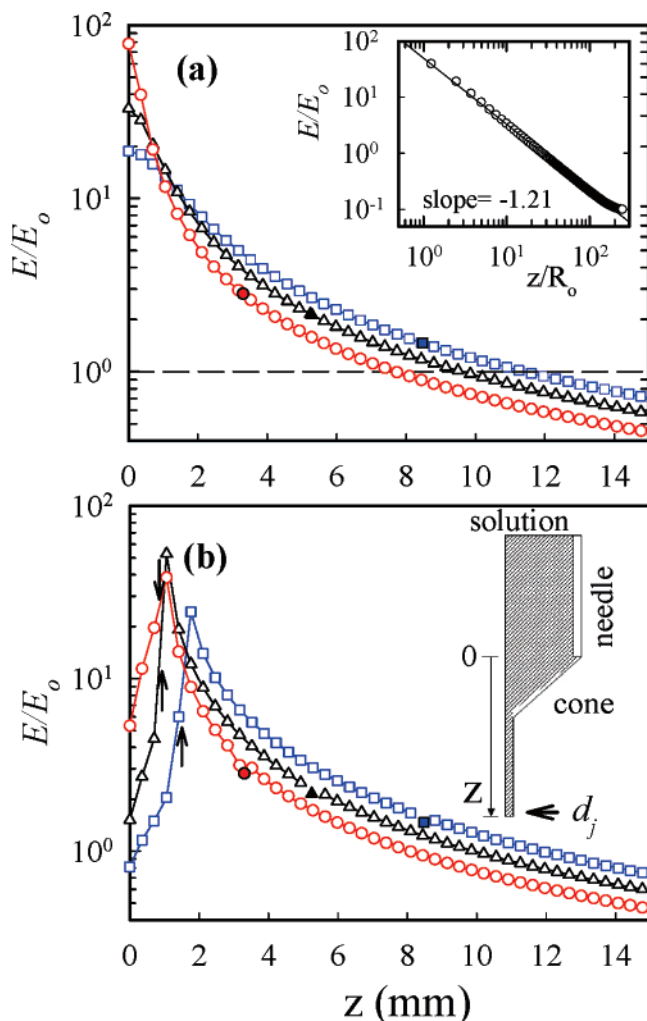

Figure 4. Calculated electric strength as a function of distance from the needle end to the grounded plate. Key: (□) ND−B needle; (△) ND−M needle; (○) ND−S needle. The filled symbols represent the position of the straight-jet end determined experimentally. (a) In the absence of liquid cone and jet. The inset shows the typical distribution of electric fields in a wide range of normalized distance, (b) in the presence of stagnant liquid cone and jet. The arrows point out the location of the cone apex determined from experiments. The nominal electric strength, E_o, is given by V/H with $V = 5$ kV and $H = 70$ mm.

solution, and a triangular Taylor cone is assumed. The locations of the cone apex and jet end, determined experimentally for different needles, are marked by the arrows and the filled symbols, respectively. It is intriguing to note that in contrast with the empty needle model (Figure 4a), the maximum electric field moves to the jet region adjacent to the cone apex, but the electric field strength at the terminal jet remains relatively unchanged. Because of a longer jet produced by the larger needle assembly (ND−B), the electric field strength that the terminal jet experiences in order to undergo the bending instability deformation is evidently smaller (ca. half of that for the ND−S needle), and thus leading to a less electrostatic stretching and

giving rise to a fatter fiber. It should be noted that our FEA calculations simply provided a first approximation of the strength of the electric field acting on the straight jet end. Because of the coupling interaction between the fluid dynamics and electrostatics, however, a more complex electric field is expected around the cone apex and the straight jet end.

Effects of PAN Concentrations. For all the adjustable electrospinning parameters, polymer concentration emerges as the most important factor in determining the diameter of electrospun fibers d_f. For the present PAN/DMF solutions at ambient temperature, γ is independent of the PAN content (∼36.3 dyn/cm), κ is slightly enhanced, but η_o is pronouncedly increased with an increase in PAN concentration. As shown in Table 3, ca. 30-fold increase in η_o but merely a 30% increase in κ are observed when the PAN concentration is doubled.

Under a condition of fixed processing variables ($Q = 0.3$ mL/h, $H = 7$ cm, and 6 kV), the effects of PAN concentrations on the cone/jet/fiber morphologies are shown in Table 3. As the solution viscosity was increased, the size of the Taylor cone remained relatively unchanged, the electrified jet became longer and relatively thicker, and PAN fibers with a larger diameter were produced. These observed trends were similar to those for the electrospinning of PS solutions reported previously.[14] When plotting the logarithm−logarithm plots of d_j and d_f vs η_o, two scaling laws exist for the present PAN/DMF solutions; that is, $d_j \sim \eta_o^{0.08}$ and $d_f = 14.8\eta_o^{0.52}$, as shown in Figure 5, where the solid circles are for the d_f and the open circles for the d_j. The weak η_o dependence of d_j is in accordance with theoretical consideration,[49] and similar results have been found on electrospinning the PS/THF solutions.[14] For the specific PS/THF solution with increasing PS contents, it should be noted that η_o was increased, but both the γ and κ were controlled to keep them constant at 24.2 dyn/cm and 1.15 μS/cm, respectively, by adding a suitable amount of LiClO$_4$ salt. In contrast, there is a ca. 30% variation in κ for the present PAN/DMF solution. Our derived exponent for the η_o dependence of d_f is in agreement with that (∼0.50) obtained by Baumgarten using a similar solution[27] and is also similar to the previously reported value for PS/THF solutions (∼0.41).[14] However, it is apparently lower than poly(methyl methacrylate)/DMF solutions (∼0.71),[10] poly(ethylene terephthalate-*co*-ethylene isophthalate)/(CF/DMF) solutions (∼0.80),[8] and Nylon-4,6/DMF solutions (∼0.86).[13] This implies that a different scaling exponent for describing the $d_f - \eta_o$ relation is applied for various solutions depending on the polymer−solvent system. When the composition of the electrospinning solution is varied, it should be reminded that not only the η_o but also the γ and κ might be altered; plausibly giving a mutual influence on the d_f determination. On the basis of the solid content, therefore, a simple relation is expressed by $d_f \sim \phi^{2.49}$ according to Figure 2a.

On the assumption that negligible solvent evaporation takes place within the electrified jet prior to reaching the bending instability region, the terminal jet velocity (v_j) can be estimated by $4Q/\pi d_j^2$ and is given in Table 3 as well. The calculated v_j is ca. 6.5−10 m/s for the 5−8 wt % PAN/DMF solutions and is

Table 3. Effects of PAN Concentration on the Solution Properties and Cone/Jet/Fiber Dimensions (Room-Temperature Electrospinning)[a]

PAN (wt %)	η_o (cP)	κ (μS/cm)	cone height (mm)	jet length (mm)	d_j (μm)	d_f (nm)	l_f/l_j	v_j (m/s)
5.0	47	35.3	1.54	1.21	3.99 ± 0.28	213 ± 47[b]		6.7
5.5	109	35.5	1.94	1.30	3.93 ± 0.20	-		6.9
6.0	171	36.0	1.49	2.24	3.25 ± 0.19	240 ± 81	8.80	10.0
6.5	194	42.8	2.13	1.37	3.78 ± 0.08	281 ± 57	9.50	7.4
7.0	338	45.4	1.25	1.88	3.84 ± 0.26	304 ± 62	9.09	7.2
8.0	515	46.2	1.49	2.80	4.04 ± 0.20	353 ± 71	8.51	6.5
10.5	1446	50.0	1.28	4.72	5.38 ± 0.23	552 ± 45	8.17	3.7
12.0	2753	51.5	1.07	12.29		1064 ± 175		

[a] γ remained constant at 36.3 dyn/cm and processing variables were fixed at $Q = 0.3$ mL/h, $H = 7$ cm, 6 kV, and the o.d. of needle is 1.47 mm. [b] Beaded fibers. d_f was determined by the fiber diameter between the spindles (beads).
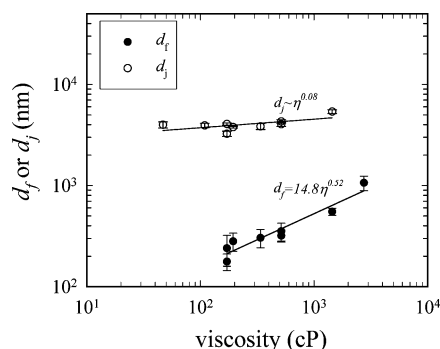

Figure 5. Viscosity dependence of jet diameter (open circles) and fiber diameter (filled circles) for PAN/DMF solutions electrospinning at ambient temperature. The solution properties are displayed in Table 3, $Q = 0.3$ mL/h, $H = 7$ cm, 6 kV, and the o.d. of the needle is 1.47 mm.

greatly reduced to 3.7 m/s for the 10.5 wt % solution; plausibly resulting from a lower effectiveness in electrostatic stretching due to the high viscosity and limited conductivity. The traveling time of the jet from the cone apex to the incipient of jet bending is extremely short (~0.2 ms), which further validates the assumption of negligible solvent evaporation. The l_f/l_j ratio associated with the jet bending is slightly reduced with the PAN content. In spite of the presence of similar jet diameter, however, our results demonstrate that the effective stretching in the bending instability region is the predominant factor that determines the final fiber diameter. In short, a whipping jet possessing a higher η_o is more difficult to be electrically stretched and eventually produces thicker fibers deposited on the grounded collector.

On the basis of the above experimental findings, the lowest diameter of PAN fibers obtained from room-temperature electrospinning was 194 ± 36 nm by using the 6 wt % solution under a processing condition of $Q = 0.6$ mL/h, $H = 7$ cm, and 7.8 kV. As mentioned previously,[18] there obviously exists a great challenge for preparing PAN fibers with a diameter less than 100 nm. To facilitate smaller fiber preparation, the temperature factor will be considered in the next section in the hope of changing the solution properties to close the gap.

3.2. Temperature Effects on Solution Properties. Shear experiments were carried out at several temperatures from 25 to 100 °C. As expected, the solution viscosity is reduced at high temperatures. It is further assumed that the temperature dependence of η_o is governed by the Arrhenius-type activation energy:

$$\eta_o(T) = \eta_o(T_o) \exp\left[\frac{\Delta E}{R}\left(\frac{1}{T} - \frac{1}{T_o}\right)\right] \quad (1)$$

where T_o is the reference temperature and R is the gas constant. Figure 6(a) shows the log η_o vs $1/T$ plots for solutions with various compositions, by which the activation energy for flow (ΔE_η) was determined from the slope and tabulated in Table 4.
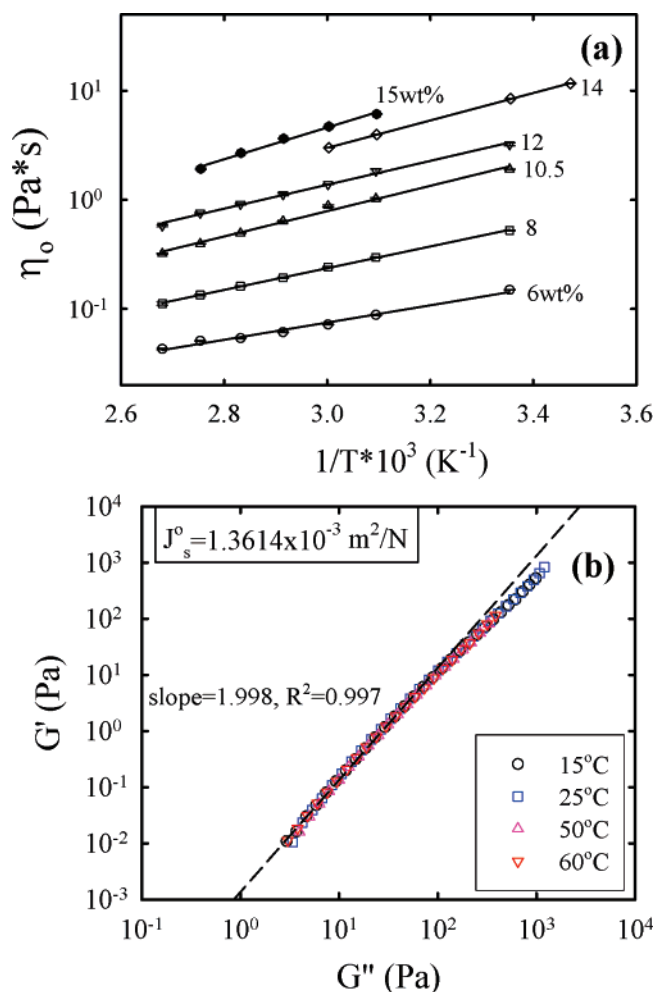

Figure 6. (a) Effects of temperature on the solution viscosity. The flow activation energy for each solution is determined from the slope, (b) Typical plot of log G' vs log G'' for the 14 wt % PAN/DMF solution at various temperatures. A master curve is constructed, suggesting the temperature independence of J_s^o.

Table 4. Activation Energy for PAN/DMF Solution Viscosity (ΔE_η), Conductivity (ΔE_κ), and Surface Tension (ΔE_γ)

PAN (wt %)	ΔE_η (kJ/mol)	ΔE_κ (kJ/mol)	ΔE_γ (kJ/mol)
6	15.1	10.9	3.02
8	19.0	10.0	3.84
12	20.9	9.8	3.95
14	24.1		
15	27.9		

The derived ΔE_η is increased with PAN concentrations, being 15.1 kJ/mol for the 6 wt % and 27.9 kJ/mol for the 15 wt % solution. Accordingly, the viscosity of the 6 wt % solution is pronouncedly decreased from 149 to 51 cP when the temperature is raised from 25 to 90 °C. Figure 6b shows the typical
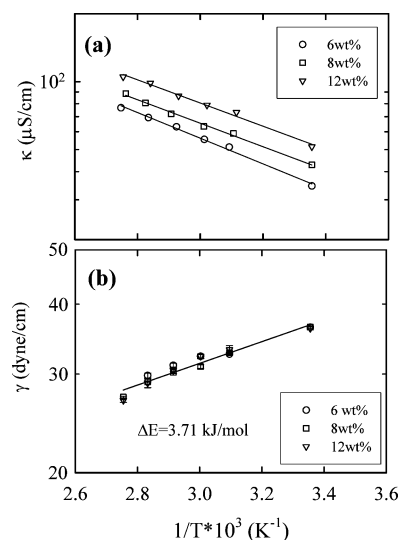
Figure 7. Effects of temperature on (a) solution conductivity, and (b) solution surface tension. The activation energy is determined from the slope.

Figure 8. Temperature effects on the voltage range for electrospinning. Filled and open squares represent the lower and upper bound voltages respectively for the stable cone−jet electrospinning mode. The inset images are cone and jet morphologies at (a) 54.3, (b) 66.9, and (c) 88.7 °C, respectively. The scale bar is 1.67 mm (12 wt % PAN/DMF solutions, $Q = 0.3$ mL/h, $H = 7$ cm, and the o.d. of the needle is 1.47 mm).

temperature effect on the log G' − log G'' plots for the 14 wt % solutions, by which J_s^o is derived from the y-intercept. A master curve is evidently formed, suggesting the solution-temperature independence of J_s^o. In other words, the entanglement density remains intact for an entangled PAN/DMF solution at different temperatures. Thus, the relaxation time depends exclusively on the solution viscosity and will be reduced for a given solution at high temperatures.

As shown in Figure 7a, the conductivity of PAN/DMF solutions increases with an increase in PAN concentrations and is also enhanced at high temperatures possibly due to the enhanced mobility. The temperature dependence of κ also follows the Arrhenius equation, and the conductivity activation energy (ΔE_κ) for each solution is determined from the slope. Also given in Table 4 is the derived ΔE_κ, showing a slightly decreasing ΔE_κ with concentrations from 10.9 kJ/mol for the 6 wt % solution to 9.8 kJ/mol for the 12 wt % solution. On the other hand, the solution surface tension is relatively independent of the PAN concentration but is decreased at high temperatures as shown in Figure 7b. The Arrhenius type of activation energy (ΔE_γ) is found to be independent of concentration, with ca. being 3.7 kJ/mol for all the solutions studied (Table 4).

On the basis of the relative values of ΔE shown in Table 4, it is evident that solution viscosity shows greater temperature dependence than the two other solution properties. Moreover, it is expected that a thinner PAN fiber should be obtained when electrospinning is performed at a higher temperature due to the favorable solution properties (i.e., lower viscosity and lower surface tension but higher conductivity) for a more significant jet stretching prior to solidification. As a matter of fact, such a phenomenon was observed, and a detailed discussion is provided in the following section.

3.3. Temperature Effects on Electrospinning. Figure 8 shows the V available at a Q of 0.3 mL/h for electrospinning the 12 wt % solution at various temperatures; also included are the typical cone and jet morphologies at an applied V of 8.9 kV. It is seen that a larger V is required for carrying out electrospinning at high temperatures than that for room-temperature electrospinning (32.2 °C). Similar results were also obtained for the 6 wt % solution. As the solution temperature was increased, the Taylor cone expanded, the jet length was monotonically shortened, and thinner PAN fibers with larger
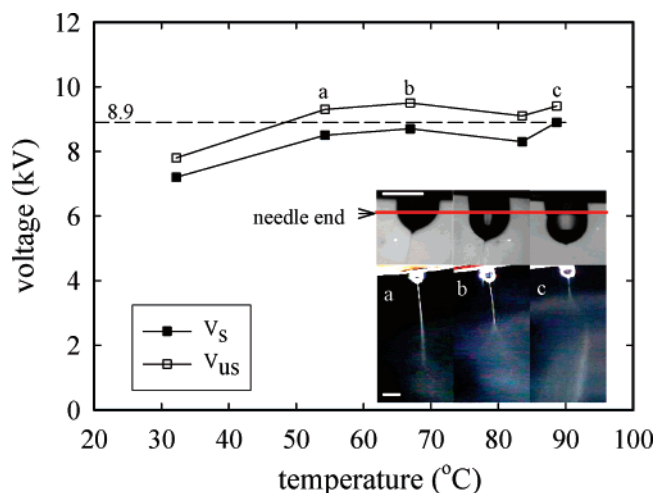
Table 5. Temperature Effects on the Cone/Jet/Fiber Morphologies, Fiber Birefringence (Δn), and Crystallinity (ϕ^{WAXD})[a]

temp (°C) 12 wt %	cone height (mm)	jet length (mm)	d_f (nm)	$\Delta n \times 10^2$	ϕ^{WAXD} (%)
32.2[b]	1.07	12.29	1064 ± 175	1.79	-
54.3	0.99	11.77	814 ± 149	1.56	11.6
66.9	1.42	7.66	651 ± 190	1.97	13.9
83.5	1.42	2.63	530 ± 308	2.05	7.0
88.7	1.48	2.34	463 ± 290	2.14	6.6

[a] Processing variables were fixed at $Q = 0.3$ mL/h, $H = 7$ cm, and 8.9 kV. The o.d. of needle is 1.47 mm. [b] $Q = 0.3$ mL/h, $H = 7$ cm, and 7.8 kV. A voltage of 8.9 kV will lead to an unstable electrospinning mode, as shown in Figure 8.

fiber birefringence were produced (Table 5). The larger V for high-temperature electrospinning is attributable to the formation of a larger Taylor cone resulting from a more conductive and less viscous PAN/DMF solution, which is consistent with the PS/DMF electrospinning results.[14] Due to the intramolecular dipole repulsions of its nitriles, PAN forms relatively stiff, rodlike molecules with a "laterally ordered" structure, but with no c-axis order. The WAXD intensity profiles of the electrospun PAN fiber mats are shown in Figure 9, where a characteristic diffraction peak at 17.2° relevant to the (200) crystal plane[33] is observed. In contrast, the powder sample gave a strong diffraction peak at $2\theta = 16.8°$. The diffraction peak was found to gradually diminish as electrospinning was performed at elevated temperatures. While birefringence detects the chain orientation within the fibers, WAXD provides the crystallinity fraction developed in the fibers by resolving the diffraction peak from the total scattering curve. The corresponding crystallinity fraction was determined and displayed in Table 5 as well. The apparent reduction of fiber crystallinity prepared from the high-temperature process is attributed to the enhanced solvent evaporation, which prohibits the chain ordering process to take place. As compared to conventional electrospinning, high-temperature solution electrospinning possesses the advantage of producing PAN fibers with a much smaller diameter and lower crystalline order, but a higher chain orientation. The TGA results of the as-spun fibers showed a weight loss of ca. 30% at 300 °C due to the cyclization of the nitrile group,[32] which was fairly consistent with the DSC heating traces exhibiting an exothermic peak at 290.9 °C with a reaction enthalpy of 500.9
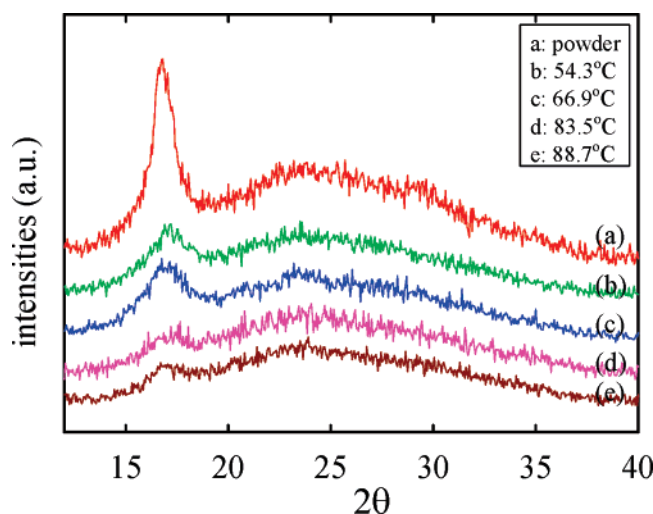
Figure 9. WAXD intensity profiles of electrospun fibers prepared from the 12 wt % solution at various temperatures ($Q = 0.3$ mL/h, $H = 7$ cm, and 8.9 kV). The crystallinity percentage of the powder sample is 18.5%.
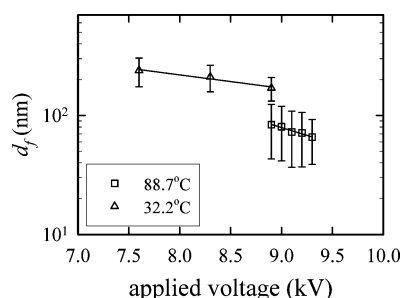

Figure 10. Effects of applied voltage on fiber diameter (6 wt % PAN/DMF solutions, $Q = 0.3$ mL/h, $H = 7$ cm).

Figure 11. Fiber morphology and the corresponding diameter distribution for the 6 wt % solution electrospun under different temperatures and voltages: (a) 32.2 °C and 8.9 kV; (b) 88.7 °C and 8.9 kV; (c) 88.7 °C and 9.3 kV. The scale bar is 400 nm ($Q = 0.3$ mL/h, $H = 7$ cm).

J/g. This resulted from the intermolecular cross-linking between PAN chains.[28,30]

To reveal the *V* effect on the cone/jet/fiber morphologies, the 6 wt % solution was electrospun at two different temperatures, 32.2 and 88.7 °C, for comparison. Under a processing condition of $Q = 0.3$ mL/h and $H = 7$ cm, the applied *V* available for the stable cone−jet mode was relatively limited, being 7.6−8.9 kV for 32.2 °C and 8.9−9.3 kV for 88.7 °C electrospinning. As the *V* was increased, both the cone height and jet length were decreased regardless of the solution temperatures, and there was a monotonic reduction of d_f as shown in Figure 10. Figure 11 shows the fiber morphology observed by SEM together with the corresponding histogram of the fiber diameter distribution. Under a fixed *V* of 8.9 kV, the diameter of the electrospun fibers was pronouncedly decreased with an increase in solution temperature. It was reduced from 170 ± 38 nm by the 32.2 °C solution electrospinning to 84 ± 41 nm for electrospinning conducted at 88.7 °C. For the present study, the smallest PAN fibers with a diameter of 65 ± 27 nm were obtained by applying the highest *V* (~9.3 kV) available for the stable cone−jet electrospinning mode at 88.7 °C.

When the solutions with various PAN concentrations (6−12 wt %) were electrospun at 88.7 °C under a processing condition of $Q = 0.3$ mL/h, $H = 7$ cm, and 9.3 kV, the cone height was found to be independent of PAN content (ca. 1.0 mm), but the jet length evidently increased from 1.1 mm for the 6 wt % to 2.0 mm for the 12 wt % solution; similar trends were also obtained from room-temperature electrospinning (Table 3). As compared to the conventional process, however, electrospinning
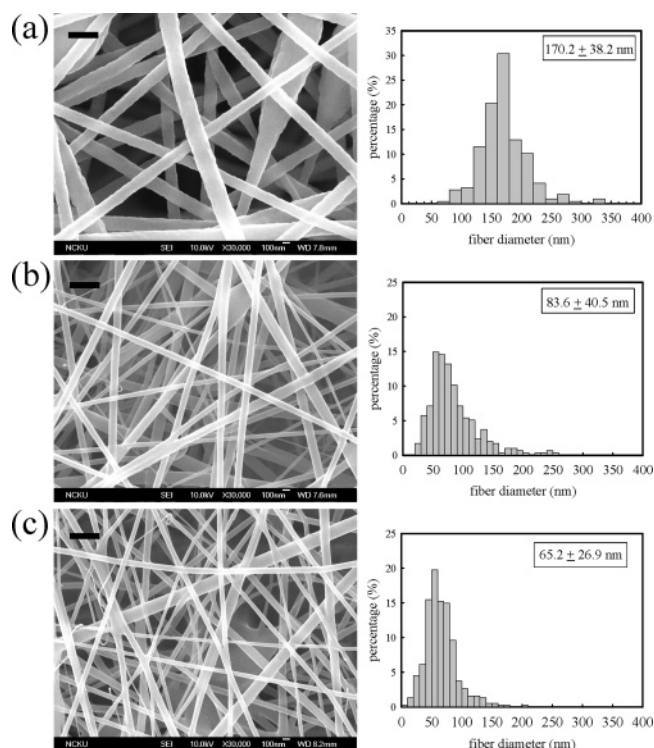
at 88.7 °C eventually produces fibers with a much smaller diameter; the values of d_f obtained from the 6 and 12 wt % solutions are 65 ± 27 and 466 ± 253 nm, respectively. Although the solution temperature is well maintained, the somewhat large standard deviation for the d_f is attributed to the absence of environmental temperature control. Because of the intensive solvent evaporation in the bending instability region, the temperature of whipping jets may tremendously drop during repulsive stretching. This cooling effect leads to a significant temperature variation from jet to jet; the variation may become more predominant for a concentrated solution electrospun at an elevated temperature. For preparing fibers with more uniform diameters, an environmental chamber has been constructed in this laboratory, and a forthcoming paper will provide the effect of environmental temperature on the fiber morphology for a complementary study.

Figure 12 shows the double logarithmic plots of d_f vs η_o for the two data sets obtained from high-temperature electrospinning; one is obtained for solutions with various PAN contents electrospun at 88.7 °C (triangle symbols with a number above data point referring to the wt% of PAN), while the other is deduced from the 12 wt % PAN/DMF solution electrospun at different temperatures (inversed triangles). Also included are the ambient electrospinning results (open symbols) taken from Figure 5. By means of linear regression analysis, the derived d_f − η_o relation for each data set is provided in Figure 12 as well. The viscosity dependence of d_f for solutions with various compositions (6−12 wt %) is found to follow the relationship of $d_f \sim \eta_o^{0.52}$ for electrospinning at 32.2 °C and $d_f \sim \eta_o^{0.74}$ at 88.7 °C. Moreover, the prefactor for the power law relation is apparently reduced as electrospinning is conducted at high temperatures. Within experimental uncertainties, it seems that the η_o dependence of d_f for high-temperature electrospinning is slightly stronger than that for room-temperature electrospinning. In deriving these scaling laws, however, one should be
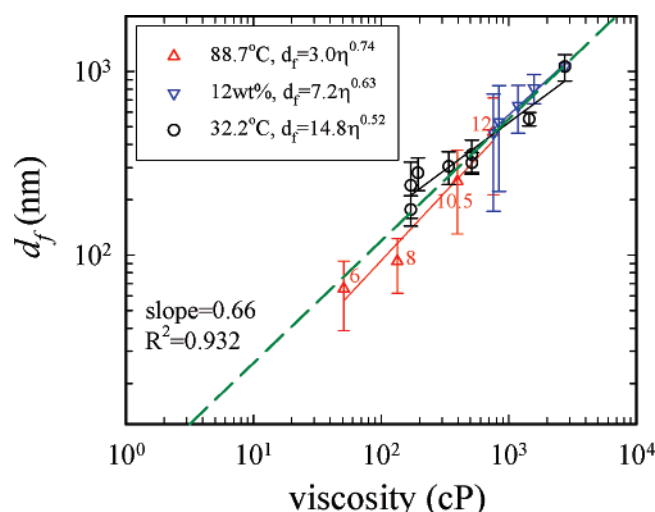
Figure 12. Solution viscosity dependence of fiber diameter. Processing variables are fixed at $Q = 0.3$ mL/h and $H = 7$ cm. Key: ($\triangle$) electrospinning at 88.7 °C for solutions with various concentrations, $\gamma \sim 26.9$ dyn/cm, $\kappa = 77-105$ μS/cm, and 9.3 kV; ($\triangledown$) electrospinning of 12 wt % solutions at various temperatures, $\gamma = 27-36$ dyn/cm, $\kappa = 52-105$ μS/cm, and 8.9 kV; ($\bigcirc$) ambient electrospinning for solutions with various concentrations, $\gamma \sim 36.3$ dyn/cm, $\kappa = 40-52$ μS/cm, and 6 kV. The dashed line is the linear regression result of all data shown.

aware of the variations of the solution properties (κ and γ) and the processing variable (V), which might lead to a coupling effect if the variation is too large. Indeed, it is extremely difficult to separate the individual η_o effect on the d_f from the others by simply changing the polymer concentration and/or temperatures without considering the parameter variations. Nevertheless, if all the data in Figure 12 are taken into the linear regression for tentative comparison, a dashed line is constructed with a derived exponent of 0.66.

4. Conclusions

In this article, the effects of needle diameter, solution properties, and processing variables on the electrospun PAN fibers have been systematically investigated and discussed. Decreasing PAN concentration and/or increasing solution temperature result in a progressive reduction of the fiber diameter. Because of the high conductivity of the PAN/DMF solutions, the dominant processing variable in determining the fiber diameter is the applied electric field, and this is in contrast with the PS/DMF solutions exhibiting a flow-rate domination.[14] As the temperature of the PAN solutions was increased, both η_o and γ were decreased, but κ was enhanced. This suggested that high-temperature electrospinning was an effective approach to significantly reduce fiber diameter through solution property manipulation. Indeed, we have presented the first experimental evidence to the best of our knowledge, that is, high-temperature electrospinning is an effective approach in producing ultrathin PAN fibers with a diameter lower than 100 nm. In contrast with the ambient process, a stronger η_o dependence of d_f is observed for high-temperature electrospinning.

References and Notes

(1) Gañán-Calvo, A. M.; Dávila, J.; Barrero, A. *J. Aerosol. Sci.* **1997**, *28*, 249.

(2) Loscertales, I. G.; Fernández de la Mora, J. In *Synthesis and measurement of ultrafine particles*; Marijnissen, J., Pratsinis, S., Eds.; Delft Univ. Press: Delft, The Netherlands, 1993; pp 115−118.

(3) Li, D.; Xia, Y. *Adv. Mater.* **2004**, *16*, 1151.

(4) Reneker, D. H.; Fong, H. *Polymeric nanofibers*; ACS Symposium Series 918; American Chemical Society: Washington, DC, 2006.

(5) Reneker, D. H.; Yarin, A. L.; Fong, H.; Koombhongse, S. *J. Appl. Phys.* **2000**, *87*, 4531.

(6) Yarin, A. L; Koombhongse, S.; Reneker, D. H. *J. Appl. Phys.* **2001**, *89*, 3018.

(7) Hohman, M. M.; Shin, M.; Rutledge, G.; Brenner, M. P. *Phys. Fluids* **2001**, *13*, 2221.

(8) McKee, M. G.; Wilkes, G. L.; Colby, R. H.; Long, T. E. *Macromolecules* **2004**, *37*, 1760.

(9) Shenoy, S. L.; Bates, W. D.; Frisch, H. L.; Wnek, G. E. *Polymer* **2005**, *46*, 3372.

(10) Gupta, P. G.; Elkins, C.; Long, T. E.; Wilkes, G. L. *Polymer* **2005**, *46*, 4799.

(11) Fong, H.; Chun, I.; Reneker, D. H. *Polymer* **1999**, *40*, 4585.

(12) Lin, T.; Wang, H.; Wang, H.; Wang, X. *Nanotechnology* **2004**, *15*, 1375.

(13) Huang, C.; Chen, S.; Lai, C.; Reneker, D. H.; Qiu, H.; Ye, Y.; Hou, H. *Nanotechnology* **2006**, *17*, 1558. On the basis of the data provided in this article, a relation between the fiber diameter and solution viscosity is derived, d_f (nm) $= 0.769\eta_o^{0.86}$ (cP), excluding the data for the beaded and ribbon-like fibers. Note that there was ca. 8% increase of κ (3800−4100 μS/cm) and 59% increase of γ (40.2−63.9 dyn/cm) as the polymer concentration was varied from 6 to 16 wt%.

(14) Wang, C.; Hsu, C. H.; Lin, J. H. *Macromolecules* **2006**, *39*, 7662.

(15) Wool, R. P. *Macromolecules* **1993**, *26*, 1564.

(16) Fetters, L. J.; Lohse, D. J.; Richter, D.; Witten, T. A.; Zirkel, A. *Macromolecules* **1994**, *27*, 4639.

(17) Takahashi, Y.; Isono, Y.; Noda, I.; Nagasawa, M. *Macromolecules* **1985**, *18*, 1002.

(18) Yu, J. H.; Fridrikh, S. V.; Rutledge, G. C. *Adv. Mater.* **2004**, *16*, 1562.

(19) Wang, M.; Yu, J. H.; Kaplan, D. L.; Rutledge, G. C. *Macromolecules* **2006**, *39*, 1102.

(20) Mit-uppatham, C.; Nithitanakul, M.; Supaphol, P. *Macromol. Chem. Phys.* **2004**, *205*, 2327.

(21) Demir, M. M.; Yilgor, I.; Yilgor, E.; Erman, B. *Polymer* **2002**, *43*, 3303.

(22) Ohkawa, K.; Minato, K.-I.; Kumagai, G.; Hayashi, S.; Yamamoto, H. *Biomacromolecules* **2006**, *7*, 3291.

(23) Li, J.; He, A.; Zheng, J.; Han, C. C. *Biomacromolecules* **2006**, *7*, 2243.

(24) Shenoy, S. L.; Bates, W. D.; Wnek, G. *Polymer* **2005**, *46*, 8990.

(25) Givens, S. R.; Gardener, K. H.; Rabolt, J. F.; Chase, D. B. *Macromolecules* **2007**, *40*, 608.

(26) Fennessey, S. F.; Farris, R. J. *Polymer* **2004**, *45*, 4217.

(27) Baumgarten, P. K. *J. Colloid Interface Sci.* **1971**, *36*, 71.

(28) Gu, S. Y.; Ren, J.; Wu, Q. L. *Synth. Met.* **2005**, *155*, 157.

(29) Gu, S. Y.; Ren, J.; Vancso, G. J. *Eur. Polym. J.* **2005**, *41*, 2559.

(30) Sutasinpromprae, J.; Jitjaicham, S.; Nithitanakul, M.; Meechaisue, C.; Supaphol, P. *Polym. Int.* **2006**, *55*, 825.

(31) Kalayci, V. E.; Patra, P. K.; Kim, Y. K.; Ugbolue, S. C.; Warner, S. B. *Polymer* **2005**, *46*, 7191.

(32) Ge, J. J.; Hou, H.; Li, Q.; Graham, M. J.; Greiner, A.; Reneker, D. H.; Harris, F. W.; Cheng, S. Z. D. *J. Am. Chem. Soc.* **2004**, *126*, 15754.

(33) Hou, H.; Ge, J. J.; Zeng, J.; Li, Q.; Reneker, D. H.; Greiner, A.; Cheng, S. Z. D. *Chem. Mater.* **2005**, *17*, 967.

(34) Ra, E. J.; An, K. H.; Kim, K. K.; Jeong, S. Y.; Lee, Y. H. *Chem. Phys. Lett.* **2005**, *413*, 188.

(35) Wang, Y.; Yang, Q.; Shan, G.; Wang, C.; Du, J.; Wang, S.; Li, Y.; Chen, X.; Jing, X.; Wei, Y. *Mater. Lett.* **2005**, *59*, 3046.

(36) Li, Z.; Huang, U.; Shang, T.; Yang, F.; Zheng, W.; Wang, C.; Manohar, S. K. *Nanotechnology* **2006**, *17*, 917.

(37) Lee, H. K.; Jeong, E. H.; Baek, C. K.; Youk, J. H. *Mater. Lett.* **2005**, *59*, 2977.

(38) Hou, H.; Reneker, D. H. *Adv. Mater.* **2004**, *16*, 69.

(39) Wang, T.; Kumar, S. *J. Appl. Polym. Sci.* **2006**, *102*, 1023.

(40) Brandrup, J., Immergut, E. H. *Polymer handbook*, 3rd ed.; Wiley: New York, 1989; pp VII/8 and VII/34.

(41) Graessley, W. W. *Viscoelastic and flow in polymeric fluids* in *Physical properties of polymers*, 3rd ed.; Cambridge University Press: Cambridge, U.K., 2004.

(42) Khodier, S. A. *Opt. Laser Technol.* **2004**, *36*, 63.

(43) Shinde, M. H.; Kulkarni, S. S.; Musale, D. A.; Joshi, S. G. *J. Membr. Sci.* **1999**, *162*, 9.

(44) Iovleva, M. M.; Smirnova, V. N.; Budnitskii, G. A. *Fiber Chem.* **2001**, *33*, 262.

(45) Larson, G.; Spretz, R.; Velarde-Ortiz, R. *Adv. Mater.* **2004**, *16*, 166.

(46) Yoon, K.; Kim, K.; Wang, X.; Fang, D.; Hsiao, B. S.; Chu, B. *Polymer* **2006**, *47*, 2434.

(47) Yu, J. H.; Fridrikh, S. V.; Rutledge, G. C. *Polymer* **2006**, *47*, 4789.

(48) Sakai, M.; Fujimoto, T.; Nagasawa, M. *Macromolecules* **1972**, *5*, 786.
(49) Gaňán-Calvo, A. M. *Phys. Rev. Lett.* **1997**, *79*, 217.
(50) Using the FLUX2D9.10 software, we have carried out the electric field calculation for the needle-to-plate configuration to reveal the effects of the needle diameter. We treated the 3-D electrostatics problem using the axisymmetric type with respect to the needle axis. The geometry of the study model was as follows: Three needles with various inner and outer diameters (given in Table 2) were studied and the length of needle was 40 mm. A grounded plate with a diameter of 600 mm was placed beneath the needle at a distance of 70 mm. Fine element meshes were built near the needle-end corner due to the presence of intense electric field, and coarse element meshes were used for the far field space. At least 20 elements beneath the needle end were constructed for a precise calculation. Within the domain of interest, ca. 6000 triangle elements were used for the finite element analysis. The relative permittivity of the air was set to be 1.0, and the potential on the needle surface and the grounded plate were set to be 5 and 0 kV, respectively, to solve the Poisson equation.